Formation of FeCl2/NaCl-nanoparticles in supercritical water investigated by molecular dynamics simulations: Nucleation rates

ARTICLE *in* PHYSICAL CHEMISTRY CHEMICAL PHYSICS · DECEMBER 2008

Impact Factor: 4.49 · DOI: 10.1039/b805725g · Source: PubMed

Formation of $FeCl_2$/NaCl-nanoparticles in supercritical water investigated by molecular dynamics simulations: nucleation rates

Norbert Lümmen*[a] and Bjørn Kvamme*[b]

Received 4th April 2008, Accepted 18th July 2008
First published as an Advance Article on the web 15th September 2008
DOI: 10.1039/b805725g

Nucleation and growth of $FeCl_2$ in supercritical water containing NaCl at different state points between temperatures of 798 and 873 K and system densities between 0.24 and 0.14 g cm^{-3} have been studied by molecular dynamics simulations. The number of NaCl ion pairs was chosen to simulate particle formation in seawater and brine of higher salinity. Rigid SPC/E water was used to model the water molecules while a combination of Coulomb and Lennard-Jones potentials was used for the ions. Two different methods for determination of nucleation rates are applied and their results compared. We find decreasing nucleation rates with both increasing temperature and decreasing system density. Our results are also compared to those we recently obtained in an investigation of pure $FeCl_2$ from supercritical water. We find both increasing nucleation rates and a decreasing size of the critical cluster with increasing amount of NaCl.

Introduction

Hydrothermal fluids are rich in various types of ions which they carry from origins below the seafloor into the oceans at hydrothermal vent sites found all over the world's oceans.[1] In a cycle, where seawater trickles away through faults and fractures in the seafloor, it is subject to changes in temperature and pressure on its way to greater depths. Contact to heat sources, like magma intrusions, can lead to a significant heating of the fluid. This can lead to an exchange of certain compounds between the hot fluid and the surrounding rock due to changes in solubility. At one point, the buoyancy of the compositionally altered fluid is so large that it streams upwards again, towards the seafloor where it vents out into the surrounding ocean water. During this cycle there are two entirely different processes which may lead to precipitation of different minerals from the dissolved ions it carries. Evaporation of water and corresponding increases in ion concentration may lead to nucleation and growth of minerals from the aqueous liquid solution. A completely different process is encountered when passing the critical point for the aqueous solution. Laboratory experiments have demonstrated that supercritical water has extremely low solubility for normal sea salts.[2] The build up of salt deposits would be a consequence. Seawater attains supercritical conditions at depths exceeding 2800 m and temperatures above 405 °C.[2] The natural domain for supercritical water on the Earth is deep in the sub-surface and inside deep-sea hot vents,[3,4] well hidden from direct observations. Thus, the only factual observations of salt precipitating from supercritical saline waters come from laboratory experiments with visual access (see for example the work of Tester *et al.*[5]). Salts may also precipitate by the boiling of seawater in subsurface or submarine settings. This was recently demonstrated by a simple laboratory experiment by Hovland *et al.*[2]

Molecular simulations are an established and valuable tool to investigate systems and processes that are difficult to observe directly by experiments due to extreme conditions like extreme heat or pressure, for example, or because they are happening on a time and length scale that is not accessible by experimental means. The simulations carried out in this investigation aim at the understanding of the first steps of salt particle formation from supercritical water. Such simulations have been carried out along with the experimental investigation by Hovland *et al.*,[6] by Sherman and Collings[7] and also recently by the authors. While the latter focused on pure NaCl[8] and pure $FeCl_2$[9] in supercritical water, we here investigate mixtures of both salts falling out from supercritical water.

Methods

Molecular dynamics simulations

We have conducted molecular dynamics (MD) simulations[10] of particle formation of $FeCl_2$ in supercritical water that also contains Na^+ and Cl^- ions at different state conditions above the critical point of water. Nucleation rates are sampled using the methods by Yasuoka and Matsumoto,[11] and the mean first passage time method by Wedekind *et al.*[12] Both methods are described below. We employ the scheme of simulation methods we used earlier in an investigation of NaCl aggregation in supercritical water at similar state conditions compared to those applied here.[8] Systems with 120 Fe^{2+} ions and 240 Cl^- ions and a number of additional Na^+ and Cl^- ions distributed in cubic simulation volumes containing 2048 rigid nonpolarizable SPC/E[13] water molecules were simulated employing the simulation package M.DynaMIX.[14]

In one set of simulations we conducted, 24 Na^+ and 24 Cl^- ions were added to the $FeCl_2$ solution to study the particle

[a] *University of Bergen, Department of Physics and Technology, Allégaten 55, N-5007 Bergen, Norway. E-mail: norbert@ift.uib.no; Fax: +47 555 89440; Tel: +47 555 82881*
[b] *University of Bergen, Department of Physics and Technology, Allégaten 55, N-5007 Bergen, Norway. E-mail: bjorn.kvamme@ift.uib.no; Fax: +47 555 89440; Tel: +47 555 83310*

formation process in supercritical seawater. In the second set of simulations 72 Na^+ and 72 Cl^- ions were added to the $FeCl_2$ solution in order to simulate the particle formation in a brine of higher salinity and study the influence of an increased amount of NaCl compared to the first set of simulations. These numbers of Na^+ and Cl^- ions in 2048 water molecules correspond to 3.7 wt% (24 NaCl) and 10.2 wt% (72 NaCl), respectively. The weight fraction of salt in seawater is 3.5 wt%.[6] A number of 120 Fe^{2+} and 240 Cl^- ions in 2048 water molecules correspond to 29.2 wt%. In the mixed $FeCl_2$/NaCl solutions studied here, the weight fractions are 28.4 wt% $FeCl_2$ and 2.6 wt% NaCl at the low NaCl concentration and 27.0 wt% $FeCl_2$ and 7.5 wt% NaCl at the larger NaCl concentration.

The rigid nonpolarizable SPC/E potential for water has proven to be reliable in calculating the properties of supercritical water[15] like critical temperature and critical density. In a comparison of static and dynamic properties of different rigid nonpolarizable water models to experimental data at ambient and supercritical conditions, Nieto-Draghi *et al.*[16] showed that the SPC/E water model performs reasonably well at conditions above the critical point and in the region where the state points studied in this investigation are located. Smith and Dang[17] investigated NaCl association in polarizable water at ambient conditions and compared their results to those obtained by using the SPC/E model for the same study. The differences in the results were minor. Brodholt[18] and Hovland *et al.*[6] used the SPC/E model successfully in studies of NaCl association at supercritical conditions in a wide range of state conditions. Brodholt[18] also pointed out that rigid nonpolarizable potential models for water tend to perform better in studies of ion association compared to polarizable models, because the dielectric constant of the solvent plays a critical role in this process and is better reproduced by the former type of models.

The simulation conditions are not exactly at the critical point or very close to it. So the differences between water models in their ability to match the phase behaviour of real water precisely is not critical. The short range characteristics of the water models play a certain role in the packing of the salts with crystal water. However, the most critical are the partial charges of the water molecules. Neither short range characteristics nor partial charges vary dramatically between the different rigid nonpolarizable water models. Thus, it is not expected that these differences will have a significant impact on the results since the coulumbic interactions between unlike charged ions will dominate the clustering kinetics.

The ion–ion and ion–water interaction was modelled by a combination of Coulomb interaction for the (partial) charges and Lennard-Jones-potantial. We used the parameter set of Smith and Dang[17] for Na^+ and Cl^- and our own for Fe^{2+} ($\varepsilon = 0.36132$ kJ mol^{-1}, $\sigma = 0.2$ nm).[19] These parameters were obtained by a fit of the potential function used here to the empirical pair potential for the Fe^{2+} ion by Curtiss *et al.*[20] We were able to reproduce the radial distribution function[20] and experimental coordination number (6 in the first solvation shell)[20] of a single Fe^{2+} ion in water at ambient conditions (298 K, 1.0 g cm^{-3}).

Start configurations for the simulations had been obtained from equilibration runs of at least 50 ps length at ambient conditions. The state conditions were changed instantly to the new temperature values of 798, 835, and 873 K and system densities between 0.14 and 0.24 g cm^{-3} by scaling the particle velocities and the simulation box dimensions as well as the particle locations within the simulation volume. No influence of the temperature and density of the system before the change in state conditions on the subsequent ion aggregation was observed. The above mentioned range of system densities was chosen to yield equilibrium pressures of about 25 MPa after the particle formation process. Periodic boundary conditions, minimum image convention and the Ewald summation-method[10] for treating long range forces were applied in all simulations. The equations of motion were integrated by a simple leap frog algorithm with a timestep of 1 fs.[21] A Nosé-Hoover thermostat[22,23] with a time constant of 100 fs was applied to keep the temperature of the water molecules at a given temperature T_{hb}. In this way, the water molecules serve not only as a solvent but also as a heat bath to the aggregating ions. By applying the thermostat on the water molecules only the dynamics of the aggregation process is not directly influenced by the velocity or momentum rescaling of the thermostat method. This approach has been successfully applied to the aggregation of NaCl[8] and $FeCl_2$[9,19] in supercritical water before.

Table 1 Stillinger criteria for the detection of clusters

Atom/ion pair	Distance/nm
Ion–ion	0.323
O–Fe^{2+}	0.32
O–Na^+	0.325
O–Cl^-	0.43
O–O	0.38

The formation of clusters was followed by use of the Stillinger criterion[24] which marks particles belonging to the same cluster if they are located within certain distances from each other. The applied distance criteria are given in Table 1 and were taken as the values of corresponding first minima of radial distribution functions.[25] Water molecules were marked as belonging to a cluster whenever the actual water molecules in consideration were neighbours to at least two ions but their number did not contribute to the cluster size. This approach has proven useful in our recent study of nucleation[9] and growth[19] of $FeCl_2$ clusters in supercritical water. If these H_2O-bridges are neglected in the cluster size detection, cluster sizes will not be determined correctly. The fact that $FeCl_2$ crystals grown from aqueous solutions contain water molecules (see, for example, ref. 26) supports this approach.

During the simulations particle coordinates and velocities were stored on disk every 0.05 ps. The simulations lasted for 50 ps but the time interval in focus here is the first 20 ps, in which most of the aggregation and first part of particle growth take place.

Nucleation

Nucleation is the first step in a phase transition, where a new phase is formed from a metastable mother phase. Density fluctuations can lead to the condensation of a liquid drop from a metastable vapour. This happens only if the density fluctuations result in large enough droplets above the so called critical cluster size, or if collisions between smaller

droplets result in rearrangements to stable droplets. Only then are the droplets individually stable enough to grow further in different ways. Surface growth or cluster–cluster collisions are the possible growth modes. The kinetic rates of these nucleation processes, and the time for clusters to reach critical size (nucleation time) depends on initial departure from equilibrium, or supersaturation. The size of the critical cluster is connected to an activation barrier, the so called critical work of formation ΔG^* (Fig. 1a). The critical cluster is either characterized by its radius r^* or the number n^* of atoms or molecules it consists of. Within the classical nucleation theory (CNT),[27,28] this work of formation is a balance between the gains in free energy obtained through the formation of the new phase and the penalties of work involved in rearranging the surroundings in order to give space for the new phase. One important assumption within CNT is that the interface between the mother phase and the new phase is sharp. This means that the properties inside the new phase are uniform and that the properties outside the new phase are uniform. This barrier is infinitely large and can not be overcome for a stable, unsaturated system (curve marked with an 's' in Fig. 1a). The activation barrier becomes smaller with increasing supersaturation and nucleation is possible by density fluctuations within the metastable system ('m' in Fig. 1a). If there is no activation barrier, like for example for an instable system ('i' in Fig. 1a), the system decomposes instantly into regions of the old and new phase. The size of the critical cluster also decreases with decreasing barrier as illustrated by the spheres of different size in Fig. 1a. Within the so called capillary approximation, the assumption is made that material properties, like for example the interface free energy, are the same for the small nucleus as for the bulk phase. This assumption is problematic when critical clusters consist just of a few atoms or molecules and the definition of its surface is not straightforward. While surface tension and interface free energy are interrelated, and the difference may be small for gas–liquid interfaces at low pressures, it is important to distinguish between these two properties in the general case. Nevertheless, despite the shortcomings of the CNT, it serves as a simple and useful model for the description of the nucleation process. Several attempts to improve it have been made and entirely new approaches have been proposed, as experimental results and predictions by the CNT can differ by many orders of magnitude for certain systems, even for the simple hard sphere system.[29] To find a dependency of nucleation rate and critical cluster size on a given supersaturation or another quantity that describes the deviation of the system from its equilibrium state at the given conditions is the main goal of all of these works.

Experimentally a supersaturated state can be achieved by a pressure or temperature jump in a vapour. Decomposition of a precursor substance or using *anti*-solvents in wet chemical processes is another possibility. Changing the solvation properties of a carrier medium, like it is easily possible in supercritical fluids like water and CO_2, can initiate particle formation and aggregation as well. Initiation of the particle formation process by changing the solvation properties of H_2O is the process we employ in our simulations.

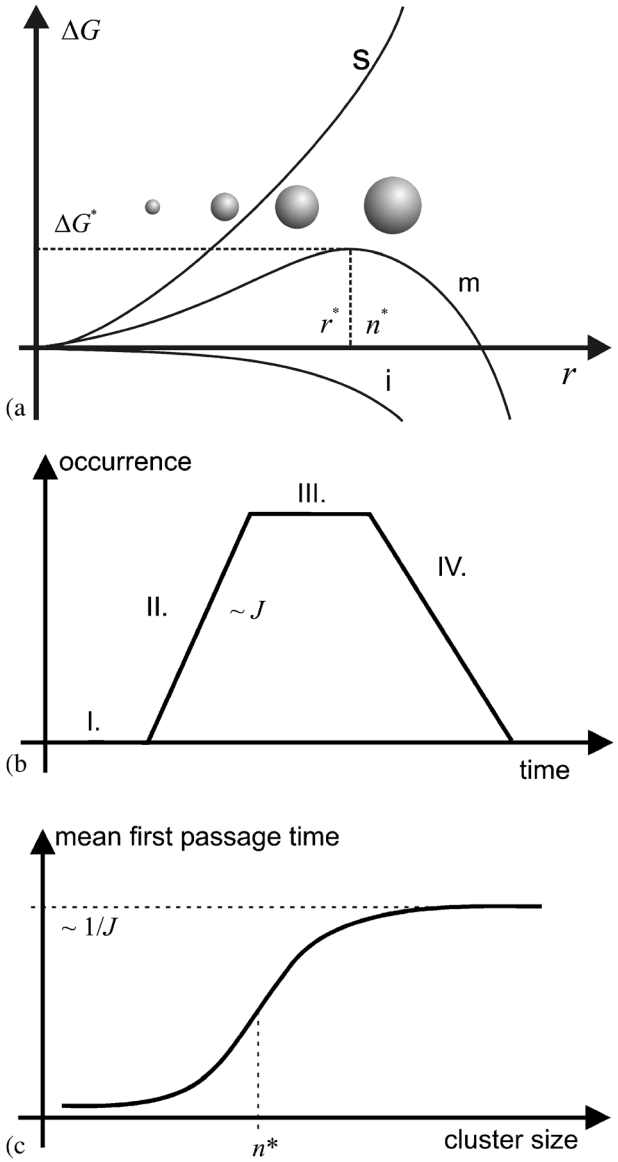

Fig. 1 (a) Work of formation ΔG *vs.* cluster radius r for a stable (s), a metastable (m) and an unstable (i) system. The activation barrier for stable cluster formation is characterized by the critical cluster size by the radius r^* or alternatively the number n^* of atoms or molecules in the critical cluster and the critical work of formation ΔG^*. (b) Schematic Yasuoka–Matsumoto diagram. (c) Schematic curve for the mean first passage time (MFPT) analysis.

Determination of nucleation rates

Method of Yasuoka and Matsumoto. The method of Yasuoka and Matsumoto (YM, ref. 11) is based on the analysis of the time development of the cluster size distribution. The nucleation rate J is the number of clusters formed within a given time and volume. To obtain it from the simulation data the cluster size distribution is calculated and the number of clusters above a selected size threshold is determined for each available configuration. A diagram like the one in Fig. 1b can be constructed in which the number of clusters above the size threshold is plotted *vs.* time. The resulting curve consists of four distinct parts. During the first

part (I), the curve is zero or shows only small fluctuations. In this time range either no cluster has yet crossed the given size threshold or those who have done so were unstable and have decayed again. A linear increase in the number of clusters above the threshold is characteristic of the second part (II) which reflects a quasistationary process of formation of new clusters. The nucleation rate can be determined from the linearly rising curve by simply dividing the slope s by the volume V of the simulation box: $J = s/V$. During the third part (III) of the curve the system has reached a stationary process of formation of new clusters and loss of clusters. This is due to growth by cluster–cluster collisions, which decreases their amount. The curve starts decaying (part IV) once there are no new clusters formed and existing clusters grow further by collisions with others. When all atoms or molecules within the system have aggregated into a single cluster the curve will eventually reach the value of one in the long time limit. This method has been successfully applied in the determination of nucleation rates of NaCl[8] and $FeCl_2$[9] in supercritical water and a variety of other systems like supersaturated water[30] and supersaturated metal vapours.[31]

Mean first passage time. The time period, which the largest cluster in a system needs to cross a certain size threshold after the change from stable to metastable state conditions, at which nucleation and growth are initiated, can also be used for the determination of nucleation rates. The so called mean first passage time (MFPT) is the key quantity in the method developed by Wedekind *et al.*[12] Furthermore, it is possible to obtain information about the size of the critical cluster. In this context we only give a brief summary and refer to the original paper of Wedekind *et al.*[12] for finer details. Within the MFPT method the probability P of a system to overcome an activation barrier is analyzed. This is achieved by taking the time derivative of the probability $P(x;t)$, where x is a reaction coordinate, in this case the number of particles n, and t is time. The height of the activation barrier is a function of the reaction coordinate as well. In the vicinity of the critical cluster size n^*, the analysis yields the equation (see ref. 12 for details):

$$\tau(n) = \frac{\tau_J}{2}(1 + \mathrm{erf}((n - n^*)c)) \qquad (1)$$

The quantity τ is the time after which the largest cluster in the system has first reached the size n, τ_J, n^* and c are fitting parameters and erf( ) is the error function. Alternatively, tanh( ) can be used which we did in this investigation. The parameter c in eqn (1) is related to the Zeldovich factor Z by $Z = c\pi^{-1/2}$ and a measure of the curvature of the activation barrier at the critical cluster size. A curve like in Fig. 1c is obtained from averages of τ from many simulation runs at the same state conditions. The size of the critical cluster n^* is located at the turning point of the sigmoidal curve, where its second derivative is zero. There, the system is on top of the energy barrier and has equal probability to 'fall' to both sides. This means that a cluster of critical size can either evaporate again on one side or become stable by further growth on the other side. The quantity τ_J, which is the value of τ where the curve levels out, is inversely proportional to the nucleation rate J. Further division by the simulation volume V yields the nucleation rate: $J = 1/(\tau_J V)$. Within the YM-method, the size of the critical cluster n^* (number of atoms in the critical cluster) must be guessed and the size threshold chosen slightly larger for determination of J. Here, it is a result of the process of fitting the equation for $\tau(n)$. At state conditions, where cluster growth follows immediately after the nucleation, the $\tau(n)$ curve does not level out and increases further. Such behaviour is likely for a very small activation barrier. Then, the fitting process can be difficult or even impossible. Fixing τ_J in the fitting process in order to impose a sigmoidal shape onto the curve within a chosen fit interval in which either the critical cluster size is expected to lie in or the time scale of the nucleation process is assumed to be is one possibility in such a case. The information obtained for the value of the critical cluster size is still valuable even if the nucleation rate is fixed in this approach. Although this method has originally been developed and tested for Lennard-Jones systems it has also been applied in investigations on nucleation in supersaturated zinc vapours[32] and in our recent study on the nucleation of pure $FeCl_2$ in supercritical water.[9]

Results

The diagrams in Fig. 2 show the typical temperature and pressure development of a few selected simulation runs. In Fig. 2a the time development of the system temperature for three systems at different heat bath temperature and different system densities is shown. Characteristic of all curves is a large increase in the system temperature after the change from ambient conditions to the supercritical state. The heat set free stems from the aggregating ions which are no longer shielded by the water molecules at these low densities. This can be seen from the curves in Fig. 2b, where the temperature development for the individual ionic species and the water molecules is plotted together with the system temperature. The ions start to aggregate immediately after the change in state conditions. During this process potential energy is converted into kinetic energy which is transferred to and removed by the water molecules, which serve as the heat bath. The heat removal does not happen instantaneously but on a time scale of about 10 ps. Fig. 2b also shows that the temperature of the Na^+ ions falls much faster towards the heat bath temperature than those of the other two ionic species.

The time development of the pressure takes longer to reach an equilibrium value. Fig. 2c shows a steep increase in pressure during the first 10 ps and then a much slower increase towards 25 MPa, for which the system densities had been selected. The curves in Fig. 2c are running averages which are shown here for easier recognition of the time behaviour of the pressure. The raw data showed larger fluctuations. The described temperature and pressure behaviour is typical for all systems we investigated.

For the calculation of nucleation rates we first analysed the simulation data with the YM-method.[11] Fig. 3 shows YM-diagrams for two systems at different state conditions with curves for four different cluster sizes as threshold values (n_{thres}). These are the same values we have used in our previous study in $FeCl_2$ nucleation. Clusters of integer multiples of three turned out to be the most abundant species in the cluster

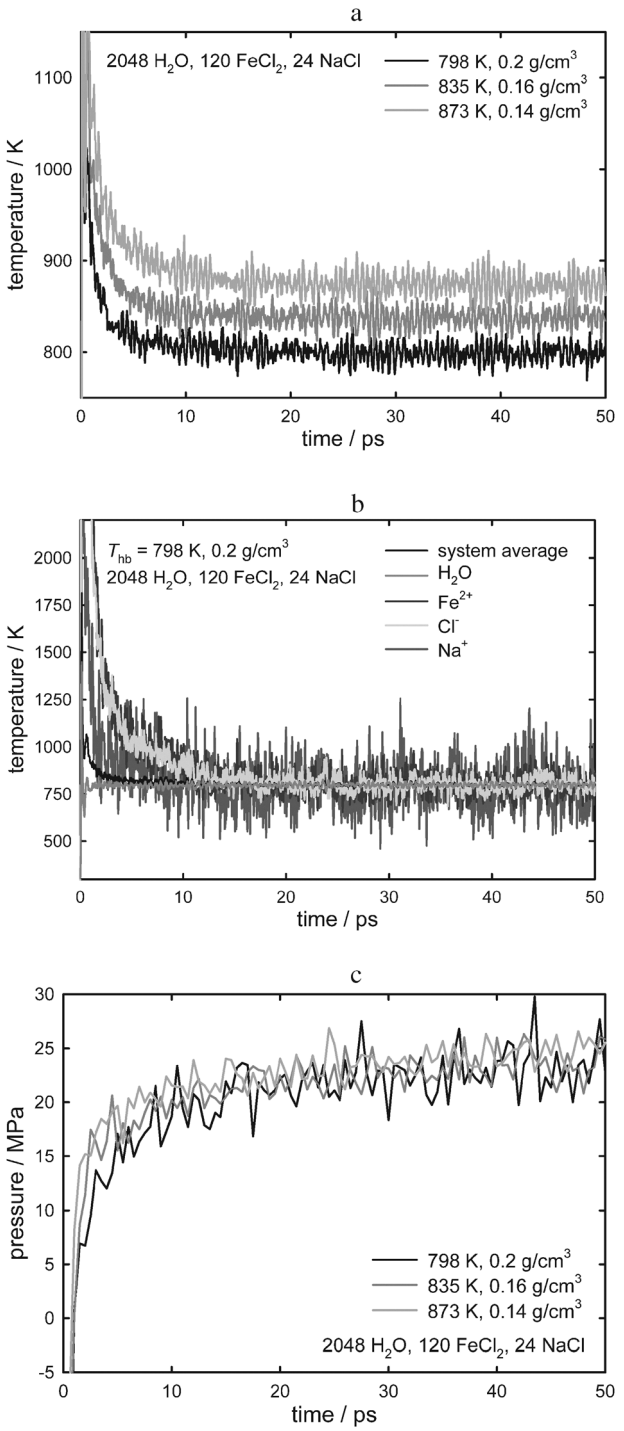

Fig. 2 (a) Time development of the system temperature for three different state points. The system contains 24 NaCl units in addition to 2048 H_2O molecules and 120 $FeCl_2$ units. (b) Temperature *vs.* time for the individual species in the simulated systems with 120 $FeCl_2$ and 24 NaCl units; (c) Time development of the system pressure for the same systems as in (a).

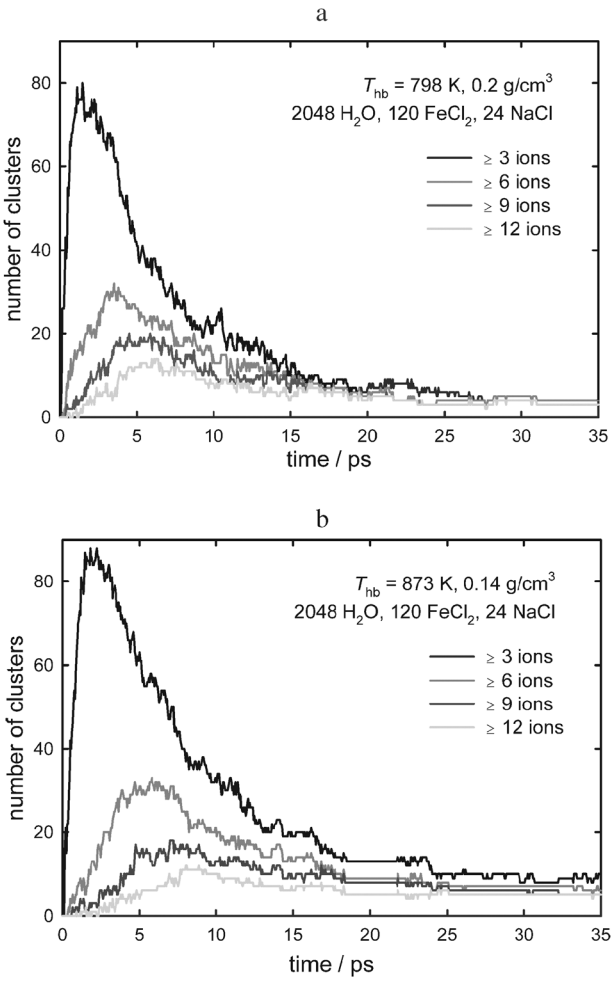

Fig. 3 Yasuoka–Matsumoto diagrams for two different systems containing 24 NaCl units in addition to 120 $FeCl_2$ units and 2048 water molecules: (a) curves for four different size thresholds in a system at 798 K heat bath temperature and 0.2 g cm^{-3} system density; (b) the same as in a for a system at 873 K heat bath temperature and a system density of 0.14 g cm^{-3}.

size distribution during the first few picoseconds of the simulations. In Fig. 3a, all four curves reach their maximum values within the first 5 ps and only those for 9 and 12 ions as threshold value show a plateau after the linear increase. This plateau is characteristic for a balance of both formation of new clusters and cluster loss due to growth by collisions of clusters larger than the size threshold. Another feature is, that the slope gets slightly smaller with increasing threshold value. In Fig. 3b, at a higher heat bath temperature and lower density, the whole process takes much longer. Although the curve for clusters of 3 ions or larger shows a similar steep increase like in Fig. 3a, the other curves rise much slower. Now also the number of clusters consisting of 6 ions or more show a plateau between about 4.5 to 7.5 ps. The slower increase of the curves is already a hint for different rates of cluster formation at different state conditions even though these rates have not yet been related to the respective simulation volumes. This has been done in the next step and the resulting nucleation rates are plotted in the diagrams of Fig. 4 while the respective data are tabulated in Tables 2 (for 120 $FeCl_2$ and 24 NaCl) and 3 (120 $FeCl_2$ and 72 NaCl). The nucleation rates are shown in relation to the average system temperature during the time interval, in which the linear slope has been determined in the YM-diagrams (Fig. 4a and b). Fig. 4a shows the nucleation

rates for the systems with 24 Na^+ and 24 Cl^- ions in addition to the 120 Fe^{2+} and 240 Cl^- ions, Fig. 4b those for the systems with 72 additional Na^+ and Cl^- ions. The different shapes of the symbols represent the three different threshold values which have been used in the analysis. Each data point is calculated from the results of 6 simulation runs at the same state conditions. Dependencies of the nucleation rate on the choice of threshold value, system temperature, system density, and number of ions per system can be found. At first, the logarithm of the nucleation rate J decreases with increasing threshold value. It also lies at smaller average system temperatures. The dependency appears nearly linearly in this half logarithmic plot. For a heat bath temperature of T_{hb} = 835 K one finds a decreasing nucleation rate with decreasing system density. This can be seen from the corresponding data points in both Fig. 4a and b. They lie closely together on the temperature axis. However, for a heat bath temperature of 798 K the behaviour is different for systems with 24 Na^+/Cl^- ions. The data points for 0.18 g cm^{-3} lie at both a higher average system temperature and larger nucleation than for 0.2 g cm^{-3} for all n_{thres}. The difference decreases on both axes with increasing value of the threshold size. For the systems with 72 Na^+/Cl^- ion pairs, the nucleation rates are much higher at 0.24 g cm^{-3} than at the lower system densities.

A comparison of nucleation rates in systems at 798 K heat bath temperature, 0.18 g cm^{-3} system density and different composition is shown in Fig. 4c. The symbol shapes represent different values for n_{thres}. The nucleation rate increases with increasing amount of NaCl for all employed threshold values. The same applies for the average system temperature during the corresponding time interval, in which J was determined.

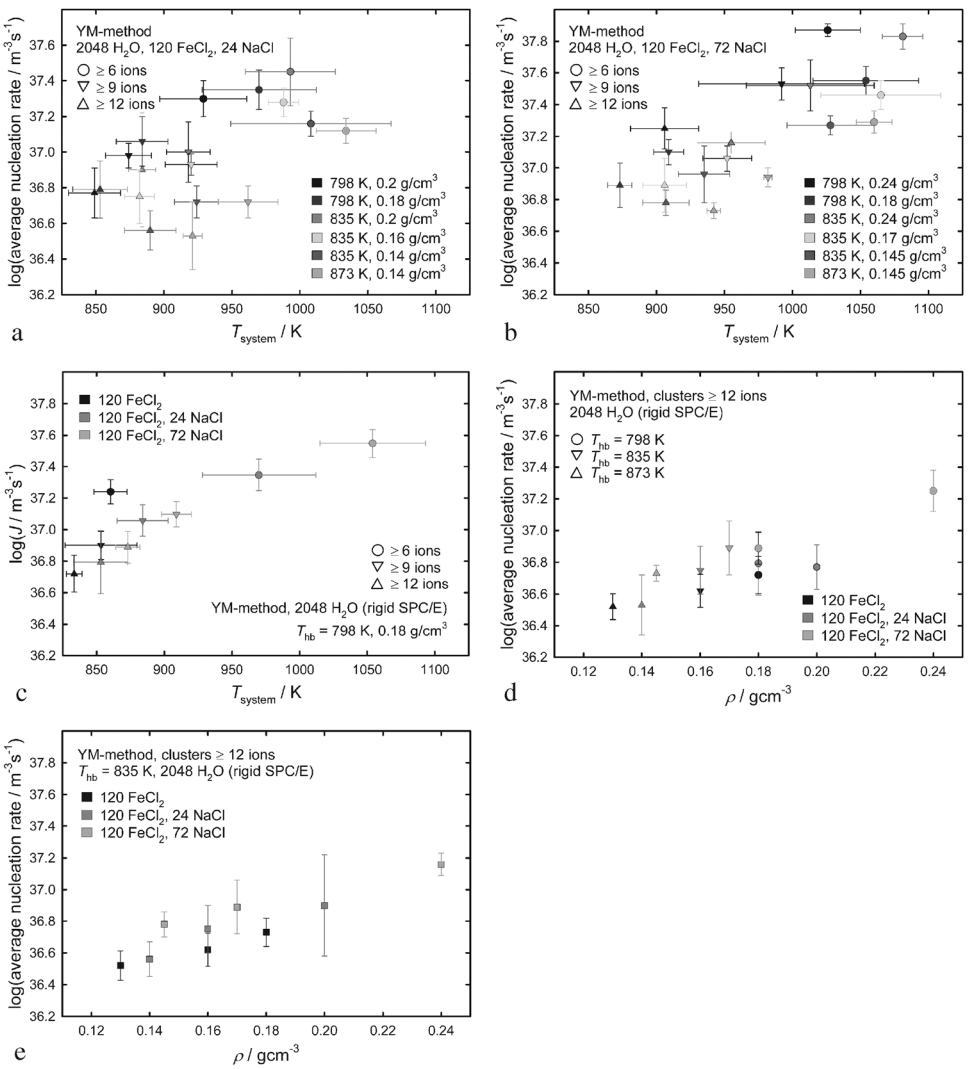

Fig. 4 To relate the data points in Fig. 4a–c to the corresponding state points we have given the heat bath temperatures (T_{hb}) in different shades of gray in the legends of these diagrams. The location of data points on the horizontal temperature axis however represents the average system temperature (T_{system}) during the time interval in which the nucleation rates were determined. (a) Nucleation rates averaged from 6 runs at the state points given in the legend. The systems contained 24 NaCl units in addition to the 2048 water molecules and 120 $FeCl_2$ units. (b) Same as in (a) but the systems contained 72 NaCl units. (c) Comparison of nucleation rates for different size thresholds for systems with different amount of NaCl in addition to water and $FeCl_2$ at a heat bath temperature of 798 K and a system density of 0.18 g cm^{-3}. (d) Same as in (c) but for different heat bath temperatures and different system densities. (e) Same as in (d) but for a size threshold of 12 ions and for different system densities at T_{hb} = 835 K.

Table 2 Data related to the Yasuoka–Matsumoto analysis of nucleation rates with different threshold values n_{thres} for the systems with 24 NaCl pairs

T_{hb}/K	ρ/g cm^{-3}	V_{box}/nm^3	n_{thres}	T/K	σ_T/K	s/ps^{-1}	σ_s/ps^{-1}	log (J/m^{-3}s^{-1})	$\sigma_{\log J}$
798	0.2	444.23	6	929	32	9.0	2.5	37.30	0.1
			9	874	17	4.2	0.6	36.98	0.07
			12	849	19	2.6	0.7	36.77	0.14
	0.18	493.59	6	970	42	11.0	2.4	37.35	0.11
			9	884	19	5.6	1.5	37.06	0.14
			12	853	20	3.1	1.0	36.79	0.16
835	0.2	444.23	6	993	33	12.6	4.6	37.45	0.19
			9	918	16	4.5	1.5	37.00	0.17
			12	884	10	3.5	1.8	36.90	0.32
	0.16	555.29	6	988	11	10.5	1.7	37.28	0.08
			9	920	19	4.7	0.6	36.93	0.06
			12	882	11	3.1	0.9	36.75	0.15
	0.14	634.62	6	1008	59	9.1	1.3	37.16	0.07
			9	924	16	3.3	0.6	36.72	0.09
			12	890	19	2.3	0.5	36.56	0.11
873	0.14	634.62	6	1034	22	8.4	1.2	37.12	0.07
			9	962	22	3.3	0.6	36.72	0.09
			12	921	7	2.1	0.7	36.53	0.19

Table 3 Data related to the Yasuoka–Matsumoto analysis of nucleation rates with different threshold values n_{thres} for the systems with 72 NaCl pairs

T_{hb}/K	ρ/g cm^{-3}	V_{box}/nm^3	n_{thres}	T/K	σ_T/K	s/ps^{-1}	σ_s/ps^{-1}	log (J/m^{-3}s^{-1})	$\sigma_{\log J}$
798	0.24	389.62	6	1026	24	29.1	3.0	37.87	0.04
			9	992	61	13.3	2.9	37.53	0.10
			12	906	25	7.0	1.9	37.25	0.13
	0.18	519.47	6	1054	39	18.3	3.4	37.55	0.09
			9	909	11	6.5	1.1	37.10	0.08
			12	873	9	4.0	1.1	36.89	0.14
835	0.24	389.62	6	1081	15	26.5	4.8	37.83	0.08
			9	1013	47	12.8	3.9	37.52	0.16
			12	955	25	5.7	0.9	37.16	0.07
	0.17	550.03	6	1065	44	16.0	3.2	37.46	0.09
			9	952	18	6.4	1.2	37.06	0.08
			12	906	16	4.3	1.4	36.89	0.17
	0.145	644.86	6	1028	32	12.0	1.6	37.27	0.06
			9	935	19	5.9	2.0	36.96	0.18
			12	907	17	3.8	0.6	36.78	0.08
873	0.145	644.86	6	1060	13	12.5	1.7	37.29	0.07
			9	982	3	5.7	0.8	36.94	0.06
			12	942	5	3.5	0.4	36.73	0.05

Fig. 4d shows a similar kind of comparison for nucleation rates in systems with different amount of NaCl. The heat bath temperature for all systems is 835 K but the system densities vary. The nucleation rate data points plotted are those for clusters of 12 ions and larger. The nucleation rates again increase with increasing amount of NaCl, even if the differences are only small as, for example, for the points at 0.13 and 0.14 g cm^{-3}. The nucleation rates increase both with increasing NaCl mole fraction and increasing density. The increase with NaCl mole fraction can be best seen for a system density of 0.18 g cm^{-3}. The diagram nearly shows a linear dependence between log J and ρ. The point at 0.2 g cm^{-3} is the only visible exception from this trend.

The diagrams in Fig. 5 show the results from the mean first passage time analysis. The data points are averages from 9 independent simulation runs at each state point. In Fig. 5a the mean first passage time for the different cluster sizes for all

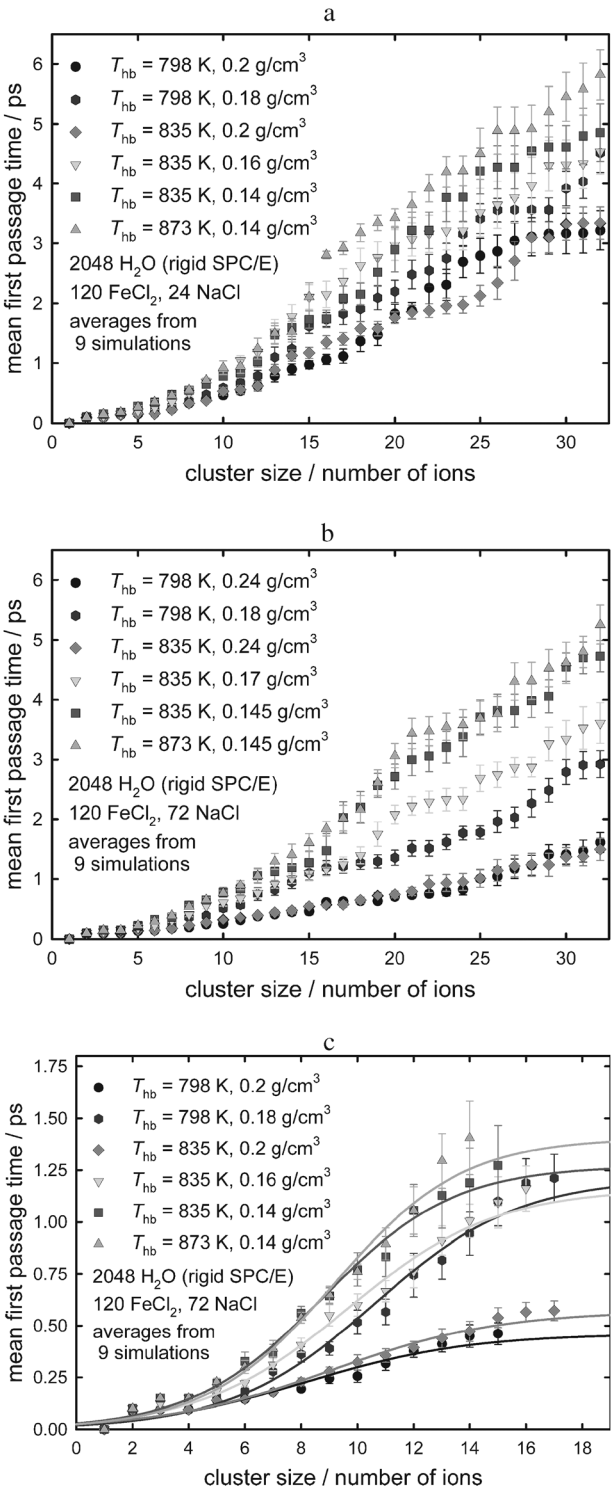

Fig. 5 (a) Mean first passage time averaged over 9 simulation runs for systems with 120 $FeCl_2$ and 24 NaCl units and the state points given in the legend. (b) Same as (a) but for the systems with 72 NaCl units. (c) Selected curves of fits of eqn (1) to the data indicated in the legend. The fit intervals have an individual size and the fits have been carried out with τ_J fixed to the mean first passage time of the largest cluster size in the fit interval (see Table 5 for the respective values).

systems containing 24 Na^+/Cl^- ions is plotted. Although the curves lie closely together until 10 ions the tendency to shorter mean first passage times for lower heat bath temperatures and higher density already shows at these small cluster sizes. This trend gets more pronounced with increasing cluster size. None of the displayed graphs shows such an ideal behaviour as in Fig. 1c which indicates that growth immediately follows the formation of stable clusters. Fig. 5b shows the mean first passage times for the systems containing 72 Na^+/Cl^- ions. The same trend concerning heat bath temperature and system density can be seen. However, the dependency of the mean first passage time on the system density is more clear here. There appear to be three groups of two curves each. The two curves at 0.24 g cm^{-3} system density lie very close together for the displayed range of cluster sizes. The second pair consists of the curves for the systems at 798 K and 0.18 g cm^{-3} and 835 K and 0.17 g cm^{-3}. Until a size of 18 ions, the curves also lie very close together and grow further at a similar rate. The different heat bath temperatures do not seem to have a significant influence on the curve development. The third pair of curves always lying closely together in the diagram are those for the two systems at 0.145 g cm^{-3} but different heat bath temperature.

In our recent analysis of the nucleation of pure $FeCl_2$ in supercritical water[19] we fitted the equation for the mean first passage time in different ways. One way was to select an individual size interval for the fit for each state point. In this way it is possible to separate the time frame of nucleation from the period of cluster growth. The individual size ranges take into account that the nucleation behaviour may be different from state point to state point. The upper limit of each fit interval, n_{max}, was chosen to be a cluster size above 12 ions and below the value where the curve showed a tendency to level out for the first time before continuing to grow further. At such cluster size, the length of the vertical error bars often starts to increase significantly, too. This indicates that a certain cluster size does not appear as often in the corresponding systems. In addition, we chose to have the parameter τ_J fixed to the value of τ at n_{max} instead of being a free parameter in the fit. We obtained more consistent results in this way and this is why we use this approach again. Fig. 5c shows an example of fit curves obtained in the described way. The results for nucleation rates and critical cluster sizes are plotted in the diagrams in Fig. 6. The corresponding data are listed in Tables 4 and 5. Fig. 6a shows a comparison of systems containing different amounts of NaCl and at both different heat bath temperatures and system densities. Independent of the heat bath temperature, there seems to be a trend to larger nucleation rates with larger system density as it had already been found with the Yasuoka–Matsumoto method. However, there is no common curvature for an imaginary curve between the corresponding data points although the behaviour seems to be monotonous for each amount of NaCl mole fraction in the three system types under investigation. At a given heat bath temperature, there is a clear behaviour of log$J$ with the NaCl mole fraction. This is indicated by the dashed lines, which group these state points in this figure and Fig. 6a and b. The size of the critical cluster for these systems, which is plotted in Fig. 6b, shows a

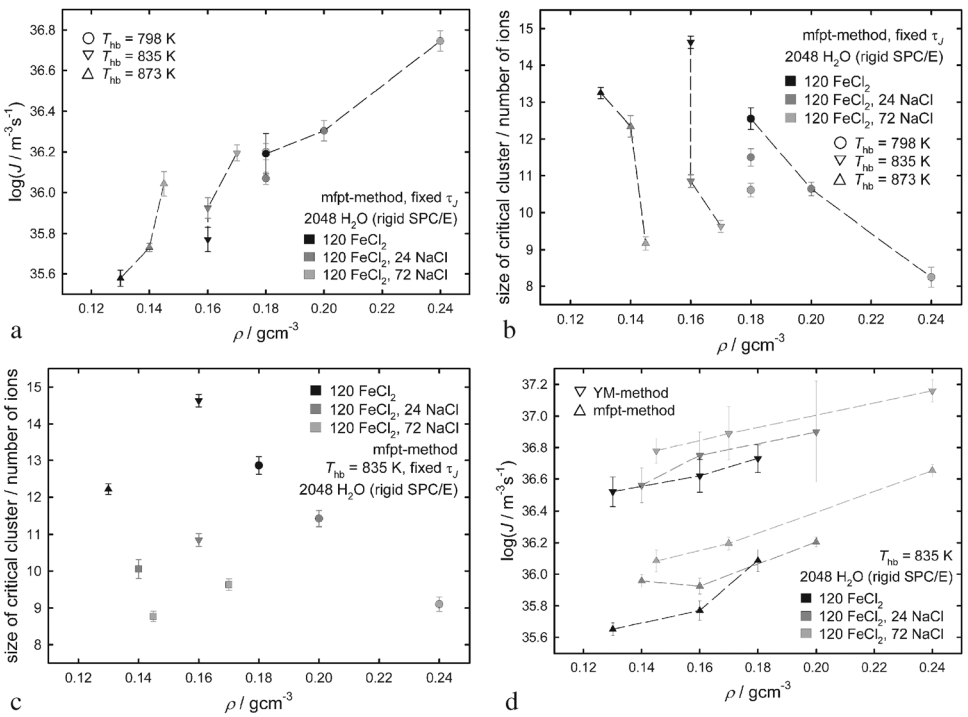

Fig. 6 (a) Logarithm of the nucleation rates as obtained by the MFPT-method with fixed τ_J for systems with different NaCl content at different state points. (b) Size of the critical cluster as obtained by the MFPT-method with fixed τ_J for the same systems as in (a). (c) Size of the critical cluster as obtained by the MFPT-method with fixed τ_J for state points at 835 K heat bath temperature but different system densities. (d) Comparison of nucleation rates obtained by the YM-method (▼) and the MFPT-method with fixed τ_J (▲) for systems at 835 K heat bath temperature, different system densities and different amount of NaCl.

Table 4 Data related to the mean first passage time analysis of nucleation rates and critical cluster sizes with different n_{max} for each state point, the systems with 24 NaCl pairs and τ_J fixed to $\tau_J(n_{max})$

T_{hb}/K	ρ_{system}/g cm^{-3}	n_{max}	n^*	c	τ_J/ps	log (J/m^{-3}s^{-1})
798	0.2	17	10.6 ± 0.2	0.19 ± 0.01	1.1 ± 0.1	36.30 ± 0.05
798	0.18	16	11.5 ± 0.2	0.22 ± 0.02	1.7 ± 0.1	36.07 ± 0.03
835	0.2	17	11.4 ± 0.2	0.21 ± 0.02	1.4 ± 0.1	36.21 ± 0.03
835	0.16	16	10.9 ± 0.2	0.23 ± 0.02	2.2 ± 0.2	35.92 ± 0.05
835	0.14	16	10.1 ± 0.3	0.21 ± 0.02	1.7 ± 0.1	35.96 ± 0.04
873	0.14	17	12.3 ± 0.3	0.19 ± 0.02	2.9 ± 0.1	35.73 ± 0.02

[1] T_{hb}: heat bath temperature; ρ_{system}: system density; n_{max}: upper boundary of fit interval (number of ions); n^*: critical cluster size; c: fit parameter; τ_J: mean first passage time; J: nucleation rate.

Table 5 Data related to the mean first passage time analysis of nucleation rates and critical cluster sizes with different n_{max} for each state point, the systems with 72 NaCl pairs and τ_J fixed to $\tau_J(n_{max})$

T_{hb}/K	ρ_{system}/g cm^{-3}	n_{max}	n^*	c	τ_J/ps	log (J/m^{-3}s^{-1})
798	0.24	15	8.2 ± 0.3	0.17 ± 0.02	0.46 ± 0.05	36.75 ± 0.05
798	0.18	17	10.6 ± 0.2	0.20 ± 0.01	1.2 ± 0.1	36.20 ± 0.04
835	0.24	17	9.1 ± 0.2	0.17 ± 0.01	0.57 ± 0.05	36.65 ± 0.04
835	0.17	16	9.6 ± 0.2	0.19 ± 0.01	1.2 ± 0.1	36.20 ± 0.04
835	0.145	15	8.8 ± 0.1	0.21 ± 0.01	1.3 ± 0.2	36.08 ± 0.07
873	0.145	14	9.2 ± 0.2	0.22 ± 0.02	1.4 ± 0.2	36.04 ± 0.06

[1] T_{hb}: heat bath temperature; ρ_{system}: system density; n_{max}: upper boundary of fit interval (number of ions); n^*: critical cluster size; c: fit parameter; τ_J: mean first passage time; J: nucleation rate

clear trend to smaller n^* with increasing amount of NaCl. However, there is no clear tendency of n^* with T_{hb} or ρ_{system} at a given composition. The values for the critical cluster sizes lie between 10.6 and 12.3 for low NaCl content and 8.2 and 10.6 for high NaCl content. Fig. 6c shows a plot of critical cluster sizes for a fixed heat bath temperature of 835 K. The trend of n^* with increasing NaCl amount is observed here as well.

Fig. 6d shows a comparison of results for the nucleation rates from both YM-method and MFPT-method for a fixed heat bath temperature of 835 K and different system densities. It can easily be seen that nucleation rates obtained by the YM method lie always above those determined by the MFPT-method. The differences are nearly up to an order of magnitude. The trend of higher nucleation rates with increasing NaCl mole fraction, as found with the YM-method, is also reflected in the MFPT-results.

The cluster size distribution and the Fe^{2+} mole fraction in clusters up to sizes of 21 ions is plotted in Fig. 7. Information on abundance and cluster composition can be obtained from such diagrams. The values in the diagrams in Fig. 7 are averages taken over 100 configurations, which represent the first 5 ps of the simulations the selected state point with T_{hb} = 798 K and ρ_{system} = 0.18 g cm^{-3} and various amounts of NaCl. In Fig. 7a the data points for monomers and dimers show increasing values with increasing amount of NaCl. The largest spread is between the data points for the amount of dimers. The values for trimers and tetramers are nearly the same for all systems. The variations from system to system

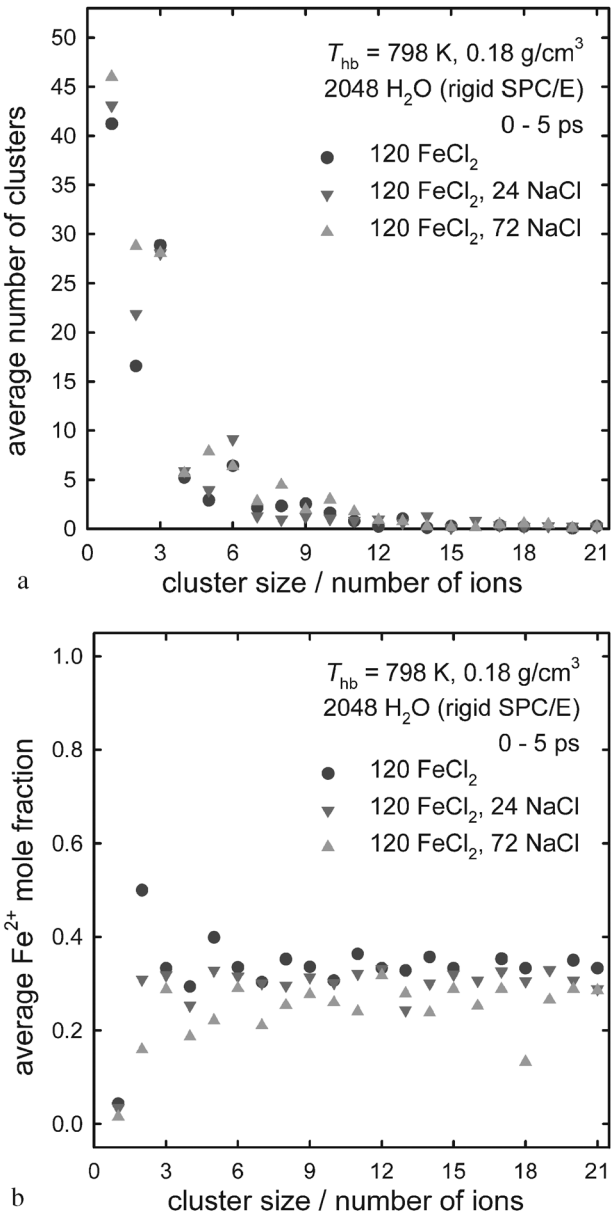

Fig. 7 (a) Cluster size distribution for the first 5 ps for systems with different amount of NaCl at 798 K heat bath temperature and a system density of 0.18 g cm^{-3}. (b) Average Fe^{2+} mole fraction of the clusters displayed in the cluster size distribution in (a).

begin with cluster sizes of 5 ions and more, while the values for clusters of size 6 ions is pronounced in all three systems. Fig. 7b shows the Fe^{2+} mole fraction of the clusters in Fig. 7a. There are only a few Fe^{2+} monomers in all three systems in the investigated time range. With increasing amount of NaCl, more and more dimers are Na^+–Cl^- dimers instead of Fe^{2+}–Cl^- dimers. The data points for the trimers lie very close to each other. However, the fact that only the value for the NaCl-free system is at 1/3 and the others lie below, hints at the existence at a few Fe^{2+}–Na^+–Cl^- trimers. The values for the clusters consisting of 6 ions lie equally close as those for the trimers which indicates mostly pure $(FeCl_2)_2$ clusters even in the systems containing NaCl. The Fe^{2+} mole fractions are more apart from each other for all cluster sizes.

The general trend for all cluster sizes is a lower Fe^{2+} mole fraction with increasing amount of NaCl with the values for the system with 24 Na^+/Cl^- ions lying much closer to those of the NaCl-free system.

Discussion

The time development of both system temperature and system pressure progresses as expected based on observations of the formation of pure NaCl particles,[8] and pure $FeCl_2$ particles[9] in our earlier studies of salt precipitation from supercritical water. However, one characteristic observation is the faster drop in temperature of the Na^+ ions compared to the other two ion sorts for the chosen NaCl concentrations. We attribute this to better coupling to the water heat bath due to the smaller ion mass.

The heat release during the initial stage of particle formation is the most likely cause for size fluctuations of the small clusters. A small cluster is in contact with fewer water molecules than a larger cluster and as a consequence the coupling to the heat bath is weaker. This can also lead to a decay of newly formed small clusters, if the potential energy transformed into kinetic energy during the collision of two or more ions or the attachment of an ion to a small cluster can not be dissipated quickly enough.

Within the YM-diagrams for the different systems one can see that the slope of the curves decrease with increasing threshold value within the analysis. As we find decreasing nucleation rates with decreasing system density with both methods we employ, it is obvious to assume that the rate of aggregation is mainly influenced by the time the ions need to travel through the system to join the next cluster. Even though there is a considerable number of monomers and dimers available during the first picoseconds after the change to supercritical state conditions, most of the building blocks are charge neutral $FeCl_2$ trimers. Their number increases almost equally fast, independent of the given state conditions. The more Na^+ ions are present, the more NaCl pairs are formed as well, as the nucleation rates are comparable for the two pure NaCl and $FeCl_2$ subsystems.[8,9] The observation that the clusters mainly aggregate from such building blocks of two or three ions instead of by successive monomer attachment could also have an influence on the slopes determined by the different selected size thresholds.

In contrast to our study on NaCl cluster formation from supercritical water, we do not relate the nucleation rates to a quantity that describes a system's deviation from equilibrium during the phase of nucleation. This is usually done by means of a system's supersaturation, which could, for example, be expressed in terms of the deviations from equilibrium concentrations at the defined density and temperature. There was no available equation of state that could describe the system properties of the investigated solutions at the given state conditions at the time this study was carried out. Furthermore, there is a whole range of supersaturations in terms of the different salts which could precipitate from the simulated solutions. It starts with the supersaturation based on the most stable solid which can precipitate at given temperature and pressure, and ends with the less stable one in terms of free energy. For these reasons we chose to relate the obtained nucleation rates to the average system temperature during the time intervals in which they were obtained during the Yasuoka–Matsumoto analysis. In case of the MFPT-analysis, the related heat bath temperature was chosen as reference.

For a heat bath temperature of 798 K and the high system densities between 0.18 g cm^{-3} and 0.24 g cm^{-3} the trend to lower nucleation rates with lower system density is different with increasing NaCl content compared to the other state points. The reason for this may be the different composition of the systems. As there is no such behaviour to be seen for the other state points it might be a composition dependent effect that shows at heat bath temperatures around and lower than 798 K and larger system densities. Further simulations at such state points could clarify this. However, an effect of the system composition can also be seen in the curves of the mean first passage times. The curves in Fig. 5a and b are much clearer separated with system density for the larger NaCl content than for the lower content. Even though the state points lie farer apart on the density scale for the higher NaCl content, the gap between the curves should increase with decreasing system density, which is the trend observed with both MFPT-method and YM-method. It is unlikely that pure NaCl nucleation dominates pure $FeCl_2$ or mixed Na^+–Fe^{2+}–Cl^- nucleation. The rates for NaCl cluster formation are comparable to those for pure $FeCl_2$ and for the combined $FeCl_2$/NaCl system.[8,9]

The analysis of the MFPT-curves with respect to the size of the critical cluster shows a distinct trend to smaller critical clusters with increasing amount of NaCl. Like for the pure $FeCl_2$ system, there is no clear trend of n^* with either heat bath temperature or system density at a certain system composition. Only a range of values for n^* can be given for each mixture of ions.

In mixed NaCl and $FeCl_2$ systems, and very likely also in others with divalent metal ions, neutral NaCl dimers and $FeCl_2$ trimers are the first stable species to be formed. However, the crucial step is the addition of further ions to such small building blocks. The stability of the smallest possible neutral unit plus one or few additional ions would be very sensitive on its composition, especially in a system, with two cations different in both size and charge. For example, as can be seen in Fig. 7b, the relative amount of Fe^{2+}–Cl^- dimers decreases with increasing NaCl content. These dimers tend to attract a further negatively charged site such as an additional single Cl^- ion, a Cl^- site in another cluster or an oxygen site in a water molecule. Size fluctuations before the start of monotonous growth are visible in the YM-curves for threshold values of both 9 and 12 ions. While size fluctuations appear also in the growth curves for much larger sizes, they are more likely to be due to rearrangements of the water molecules surrounding the clusters. During such rearrangements the distances between the nearest ions of the colliding clusters, or those bridged by a common H_2O molecule, are pushed beyond the distance of the corresponding Stillinger criterion. Those size fluctuations of clusters smaller than about 12 ions are more likely to be caused by structural instabilities due to the strong ionic charges. We therefore chose to have the upper boundary of the fit interval at least

12 ions. The value for n_{max} was then picked as the cluster size, for which the systems illustrated in Fig. 5a and b showed tendencies to level out for the first time or where the transition to further growth was assumed to happen. As the MFPT-method tends to overestimate the size of the critical cluster in cases where growth immediately follows nucleation[32] the actual sizes of the critical cluster could be lower than the fitted results indicates for the investigated systems as well. The obtained range of critical cluster sizes of 10–13 ions (120 $FeCl_2$, 24 NaCl) and 8–11 ions (120 $FeCl_2$, 72 NaCl) fit well into the picture of the critical cluster size being larger than the smallest stable neutral ion pairs and tripletts. The direct observation in the data files showed that the largest cluster in the system may often be subject to decay up to sizes of about 12 ions and tended to grow when this size was exceeded. The increasing amount of small and charge neutral NaCl clusters could have a stabilizing effect on the clusters containing Fe^{2+} ions. This could explain the decreasing critical cluster size with increasing NaCl content.

The number of simulation runs carried out and used in the curve fitting is relatively low compared to the amount of simulations used in the original work.[12] However, as the nucleation and growth of particles starts immediately after the change to supercritical conditions and the ion aggregation happens due to the strong coulombic charges and their reduced shielding by the water ions, the barrier to nucleation is expected to be extremely low. Therefore, the average time when a certain cluster size is obtained is much less dependent on the number of simulations runs necessary for good statistics than in systems with comparably weaker interactions, like Lennard-Jones systems, for example. The average time to form the first stable cluster to cross the nucleation barrier varies much more from simulation run to simulation run in such weakly interacting systems than it is the case for the systems under investigation here.

An additional reason for the shape of the obtained MFPT-curves and their growth behaviour is expected to lie in the fact, that cluster growth by collision of stable dimers and trimers is more likely than attachment of single ions. The MFPT-method has been originally developed for Lennard-Jones system in which such stable units of two or three atoms (and integer multiples of these) are not that abundant as in the investigated ionic systems. We assume that this is also a cause for the unclear behaviour in the analysis of the critical cluster size by means of the MFPT-method at a given system composition. The question is if the τ_J and n^* values obtained from a fit would improve, if one would use an offset on the mean first passage time axis for the smallest stable unit in case of systems like we investigated here. The two smallest stable species would obviously be a NaCl molecule and a $FeCl_2$ molecule. These molecules are formed very quickly and in large amount so that a large part of the further aggregation of subcritical clusters and clusters larger than the critical cluster sizes goes *via* condensation of further ions on these smallest stable building blocks and collisions of these smallest stable species. A time offset taking into account the very quick formation of stable and charge neutral dimers and trimers would lead to a smaller mean first passage time and as such further close the gap found between the values of the nucleation rates between the MFPT-method and the method of Yasuoka and Matsumoto.

Conclusions

The formation of salt particles in a mixture of Na^+, Fe^{2+} and Cl^- ions in supercritical water has been investigated by molecular dynamics simulations. The nucleation rates obtained by two different methods (Yasuoka–Matsumoto-method, MFPT-method) lie on the order of 10^{35} m^{-3} s^{-1} to 10^{37} m^{-3} s^{-1}. The trend to larger nucleation rates with increasing NaCl content shows up in the analysis independent of the method applied. The obtained nucleation rates in the mixed $FeCl_2$/NaCl systems are both comparable and larger than those of pure NaCl and $FeCl_2$ in supercritical water. The critical cluster size is found to lie on the order of 8 to 13 ions using the MFPT-method. As growth follows immediately on nucleation, we assume the actual critical cluster sizes to be a few ions smaller than the sizes obtained by the MFPT-method.

Acknowledgements

This work was financially supported by the Deutsche Forschungsgemeinschaft (DFG) by a research scholarship for NL (grant NL-1406-1/1).

All simulations were carried out on the Linux cluster 'fimm' at the Bergen Center for Computational Science (BCCS, http://www.bccs.uib.no) in Bergen, Norway.

References

1 R. P. Lowell, P. A. Rona and R. P. Von Herzen, *J. Geophys. Res.*, 1995, **100**(B1), 327.
2 M. Hovland, H. G. Rueslåtten, H. K. Johnsen, B. Kvamme and T. Kuznetsova, *Mar. Pet. Geol.*, 2006, **23**, 855.
3 K. L. Von Damm, M. D. Lilley, W. C. Shanks III, M. Bockington, A. M. Bray, K. M. O'Grady, E. Olson, A. Graham and G. Proskurowski, *Earth Planet. Sci. Lett.*, 2002, **206**, 365.
4 Y. Kawada, S. Yoshida and S. Watabane, *Earth Planets Space*, 2004, **56**, 193.
5 J. Tester, H. R. Holgate, F. J. Armellini, P. A. Webley, W. R. Killilea, G. T. Hong and H. E. Berner, Supercritical water oxidation technology, in *Emerging technologies in hazardous waste management III*, American Chemical Society, 1993, pp. 35–76.
6 M. Hovland, T. Kuznetsova, H. G. Rueslåtten, B. Kvamme, H. K. Johnsen, G. E. Fladmark and A. Hebach, *Basin Res*, 2006, **18**, 221.
7 D. M. Sherman and M. D. Collings, *Geochem. Trans.*, 2002, **3**, 102.
8 N. Lümmen and B. Kvamme, *Phys. Chem. Chem. Phys.*, 2007, **9**, 3251.
9 N. Lümmen and B. Kvamme, *J. Supercrit. Fluids*, 2008, DOI: 10.1016/j.supflu.2008.07.017.
10 M. P. Allen and D. J. Tildesley, *Computer Simulation of Liquids*, Oxford University Press, Oxford, UK, 1989.
11 K. Yasuoka and M. Matsumoto, *J. Chem. Phys.*, 1998, **109**, 8451.
12 J. Wedekind, R. Strey and D. Reguera, *J. Chem. Phys.*, 2007, **126**, 134103.
13 H. J. C. Berendsen, J. R. Gridera and T. P. Stratsmaa, *J. Phys. Chem.*, 1987, **91**, 6269.
14 A. P. Lyubartsev and A. Laaksonen, *Comput. Phys. Commun.*, 2000, **128**, 565.
15 T. M. Hayward and I. M. Svishchev, *Fluid Phase Equilib.*, 2001, **182**, 65.
16 C. Nieto-Draghi, J. Bonet Avalos and B. Rousseau, *J. Chem. Phys.*, 2003, **118**, 7954.
17 D. E. Smith and L. X. Dang, *J. Chem. Phys.*, 1994, **100**, 3757.
18 J. P. Brodholt, *Chem. Geol.*, 1998, **151**, 11.

19 N. Lümmen and B. Kvamme, *J. Phys. Chem. B*, 2008, DOI: 10.1021/jp710156b.
20 L. A. Curtiss, J. Woods Halley, J. Hautman and A. Rahman, *J. Chem. Phys.*, 1987, **86**, 2319.
21 R. W. Hockney, *Meth. Comput. Phys.*, 1970, **9**, 136.
22 S. Nosé, *Mol. Phys.*, 1984, **52**, 255.
23 G. J. Martyna, D. J. Tobias and M. L. Klein, *J. Chem. Phys.*, 1994, **101**, 4177.
24 F. H. Stillinger, *J. Chem. Phys.*, 1963, **28**, 1486.
25 N. Lümmen and B. Kvamme, in preparation.
26 D. D. Thornton, *Phys. Rev. B: Solid State*, 1970, **1**, 3193; J. N. McElearney, H. Forstat and P. T. Bailey, *Phys. Rev.*, 1969, **181**, 887.
27 M. Volmer and A. Z. Weber, *Z. Phys. Chem.*, 1926, **119**, 277.
28 R. Becker and W. Döring, *Ann. Phys.*, 1935, **24**, 719.
29 L. Granasy, T. Pusztai, G. Toth, Z. Jurek, M. Conti and B. Kvamme, *J. Chem. Phys.*, 2003, **119**, 10376.
30 K. Yasuoka and M. Matsumoto, *J. Chem. Phys.*, 1998, **109**, 8463.
31 N. Lümmen and T. Kraska, *Eur. Phys. J. D*, 2007, **41**, 247.
32 F. Römer and T. Kraska, *J. Chem. Phys.*, 2007, **127**, 234509.